immunofluorescence or immunohistochemical staining, using antibodies for C4d and/or C3d which are complement fragments, within the endothelial layer. Infrared (IR) imaging derives chemical information from inherent biochemistry, giving a measure of levels of biomolecular components (DNA, RNA, carbohydrates, proteins, etc). IR imaging can help classify disease states. In this study, we use IR imaging to find a fingerprint of AMR, and correlate it with immunohistochemical staining for C4d.
Design: Three study groups were created: native heart biopsies (from heart failure patients), transplanted hearts with positive AMR, and transplanted hearts with negative AMR by C4d staining. Each group had five biopsies. Multiple sections were cut: Hematoxylin and Eosin, C4d, CD31, and one unstained for IR imaging. Fourier Transform Infrared (FT-IR) and Quantum Cascade Laser (QCL) were used for IR imaging. Using the multiple stains, regions of interests (ROI) were selected on the IR image: myocardial and endothelial cells. Multivariate analysis and a classifier were used to see how the three groups compared.
Results: Principal component analysis (PCA), a multivariate analysis, was used to find the inter-sample variance across samples and showed grouping within each group. Linear discriminate analysis (LDA), a classifier, was able to separate patients into their respective groups. We were able to find that there was a biochemical difference of AMR positive compared to the other two groups. Myocardial ROIs had a better separation than endothelial ROIs.
Conclusions: In this study, we demonstrated that AMR positive biopsies had a unique fingerprint different from AMR negative and native hearts. Myocardial cells had better separation than endothelial cells, which may indicate AMR affects the whole heart instead of just endothelial cells. IR imaging is a novel tool in the clinical setting of pathology and has the potential to fit into current clinical workflow.

2118 Clinical Experiences of a Custom 68-Gene NGS Panel for Molecular Testing in Solid Tumors

Danbin Xu, Hye Son Yi, Shruti Bhide, Christopher Lunter, Andre Rivera, Anna Berry. CellNetix Pathology & Laboratories, Seattle, WA; Symbiodx, Seattle, WA.
Background: Next-Generation-Sequencing (NGS) enables efficient and cost-effective analysis of a number of cancer-related genes simultaneously to facilitate the clinical decision in cancer diagnosis, prognosis, and treatment management. A 68-gene panel with over 600 amplicons covering more than 4000 potential variants have been developed and validated in our laboratory. Application of this NGS panel complimentary to the anatomic pathology service demonstrates clear clinical benefits for cancer patients.
Design: A standard operating procedure was established through our extensive in-house validation process by using 69 DNA samples extracted from 58 FFPE tissue blocks and 11 whole blood specimen. FFPE tissue sections were reviewed by an onsite pathologist and manually micro-dissected to determine/improve the tumor load. Genomic DNA was used for amplification of targeted regions (Illumina TruSeq Custom Amplicon) and subsequent sequencing analysis on MiSeq using V3-600 chemistry. The raw VCF data is independently analyzed for the presence of any essential actionable mutations, read-depth of the targeted regions, and specimen-specific variants through an in-house developed filtering algorithm. A streamlined bioinformatics pipeline was established and was implemented into the data analysis of clinical specimen.
Results: A total of 216 solid tumor specimens have been tested for this 68-gene panel in the past few months. Lung, colorectal, and breast adenocarcinomas represented the majority of the tumor types being tested which account for 19%, 12.5% and 12% respectively. The average read depth for the target regions is approximately 2,000X to 2,500X and the limit of detection of this assay is at approximately 5% to 10% of the minor allele against the major allele background based on the overall tumor loads of the specimens. Over 800 aberrations have been reported out for the specimen being tested and approximately half of these variants have been reported in the literature. TP53, KRAS, APC and PIK3CA are among the most frequently mutated genes in the specimen tested. Both clinical actionable mutations and clinical applicable mutations have been identified in the same tumor specimen in multiple cases.
Conclusions: Our comprehensive 68-gene NGS panel is a sensitive and specific assay for the hotspot mutations analysis. It provides a highly efficient approach to clinical laboratory for routine molecular oncology testing and additional therapeutic options to cancer patients.

2119 ALK Immunocytochemistry on Cell-Transferred Cytologic Smears of Lung Adenocarcinoma

Chen Zhang, Melissa Randolph, Kelly Jones, Harvey Cramer, Liang Cheng, Howard Wu. Indiana University School of Medicine, Indianapolis, IN.
Background: Anaplastic lymphoma kinase (*ALK*) gene rearrangement defines a subgroup of lung adenocarcinoma that may be successfully treated with the ALK inhibitor crizotinib. ALK immunohistochemical staining (IHC) performed on formalin fixed paraffin embedded tissue or cell blocks (CB) has been reported as an effective and affordable alternative to fluorescence hybridization in situ (FISH) for the detection of *ALK* gene rearrangement. However, cytology smears frequently constitute the only available source of tumor cells due to insufficient CB cellularity. This study is aimed to assess the utility of ALK immunocytochemical staining (ICC) on direct smears using the cell transfer (CT) technique for the detection of *ALK* rearrangement.
Design: Fine needle aspiration (FNA) cases diagnosed as primary or metastatic lung adenocarcinoma in which the status of *ALK* rearrangement had been determined by FISH performed either on CB or concurrent surgical biopsies were identified over a period of 24 months. ICC staining for ALK (clone D5F3) was performed on alcohol-fixed Papanicolaou-stained direct smears using the CT technique. ALK immunoreactivity was evaluated in a modified semiquantitative graded criteria as: score 3+ for strong, granular cytoplasmic staining in most of tumor cells; score 2+ for moderate, smooth cytoplasmic staining in most of tumor cells; score 1+ for faint, focal cytoplasmic staining; and score 0 for complete absence of staining. Scores 2+ and 3+ were reported as positive and scores 1+ and 0 were reported as negative. These ICC results were compared with the corresponding FISH data from the same patients.
Results: A total of 42 FNA specimens from 42 patients were included in this study. 36 were negative and 6 were positive for *ALK* rearrangement on FISH. Four of 6 FISH positive cases showed positive ALK ICC staining (66.7%) and 35 of 36 FISH negative cases were negative on ALK ICC staining (97.2%). The overall correlation between ALK ICC and FISH was 92.9%. The two ICC-/FISH+ cases had low cellularity on direct smears which may account for the false negative results by ICC. The one ICC+/FISH- case had an ICC score 3+.
Conclusions: ICC performed on FNA smears using the CT technique is an acceptable alternative method for assessing *ALK* rearrangement, especially when the direct smears are highly cellular and the CB lacks adequate cellularity.

Ultrastructural Pathology

2120 Undifferentiated Embryonal Sarcoma of Liver in Adult: Unique Ultrastructural Features and Immunophenotypes

Andrew Bandy, Haonan Li, Xiaoming You, Yihe Yang, Jie Liao, MS Rao, William Laskin, Guang-Yu Yang. Northwestern University, Chicago, IL.
Background: Undifferentiated embryonal sarcoma (UES) of the liver is a rare malignancy that occurs predominantly in children, with few reports in adults. The tumor is dominantly composed of primitive mesenchymal elements with few differentiating features. Such morphologic undifferentiated features lead diagnostic difficulty, particularly due to lack of definitive immunostaining, which most times require large, expensive immunostaining panels to be performed. We studied a cohort of liver UES in adults, using electron microscopy (EM) and a panel of immunohistochemical stains to determine tumor cell lineage.
Design: Three cases of UES in the liver were obtained from our institutional pathology database, two found in 17-year old females and one found in a 34-year old female. Histological, immunohistochemistical and ultrastructural studies were employed for all cases.
Results: Morphologically, all three tumors showed a pseudocapsule partially separating the normal liver from undifferentiated sarcomatous cells. Two cases displayed densely cellular areas of predominantly spindle cells and myxoid, paucicellular areas with stellate and spindled cells. Rare large tumor cells with prominent hyaline globules were also seen. One case showed similar morphologic features but had prominent anaplastic/bizarre tumor cells with rhabdoid features and hyaline globules. Ultrastructural studies revealed a background of amorphous collagen-poor matrix containing polygonal cells with a high nuclear to cytoplasmic ratio with abundant organelles, but absence of intracytoplasmic filaments, filament-ribosomal complexes or any other differentiating elements. Degenerative lysosomes were identified in occasional bizarre cells. Immunohistochemical phenotyping demonstrated neoplastic cells were positive for vimentin in all three cases and 2 of the three cases showed positive staining for CD56. One case showed positivity for glypican 3 or desmin. The large tumor cells with prominent hyaline globules showed positivity for D-PAS and CD68. All tumor cells were negative for S100, melan A, myogenin, myoD1, muscle actin and smooth muscle actin, c-kit, DOG-1, CD10, CD99, CD34, Bcl-2, HePar-1, cytokeratin Cam5.2 and AE1/AE3, and EMA.
Conclusions: Our results further support the undifferentiated nature of this tumor and origin from primitive mesenchyme. Although large and expensive immunostaining panels are necessary and function to exclude any potential differentiation, electron microscopy appears to be a unique approach for diagnosis and helps to determine differentiation in the tumor for proper classification.

2121 Human Immunodeficiency Virus in Glomerular Epithelial Cells in HIV-Associated Nephropathy

Xin Gu, Kunle Ojemakinde, Guillermo Herrera. Louisiana State University Health Sciences Center, Shreveport, LA.
Background: HIV-associated nephropathy (HIVAN) is an aggressive kidney disease in HIV-1-infected patients. HIVAN is characterized by the collapse of the glomerular tufts, epithelial (podocyte) hypertrophy/hyperplasia and diffuse foot process effacement with concurrent tubular microcystic dilation and tubulointerstitial nephritis. Podocytes injury is believed a major cause for glomerular morphologic changes in HIVAN.
Both human and animal studies have indicated that glomerular podocytes are not permissive to HIV-1 replication, and pathological changes of podocytes are caused by their exposure to HIV proteins rather than direct virus infection. We are not aware of any previous report of HIVAN that described virus infection and replication in the podocytes in human kidney biopsies. In here, we provide an electron microscopic evidence of HIV infection and replication in podocytes in associated with cellular injury in an HIV patient.
Design: Kidney biopsy tissue was prepared for light microscopy, immunofluorescence and electron microscopy following routinely protocol that is applied for medical renal disease.
Results: The biopsy has 24 glomeruli, 10 of them are sclerotic. Collapsing and usual type segmental sclerosis is seen in 8 viable glomeruli. Interstitial inflammation and tubular microcystic dilation are present. The immunofluorescence study is negative for all reactants. Electron microscopy shows diffuse effacement of foot processes, segmental collapse of glomerular tufts associated with podocyte hyperplasia and fragmentation of cytoplasm. Packed viral particle are present in intact (figure A, B, arrows) as well as fragmented podocytes (figure C, D). The shape and size of viral particles are similar to previously described in infected lymphocytes.

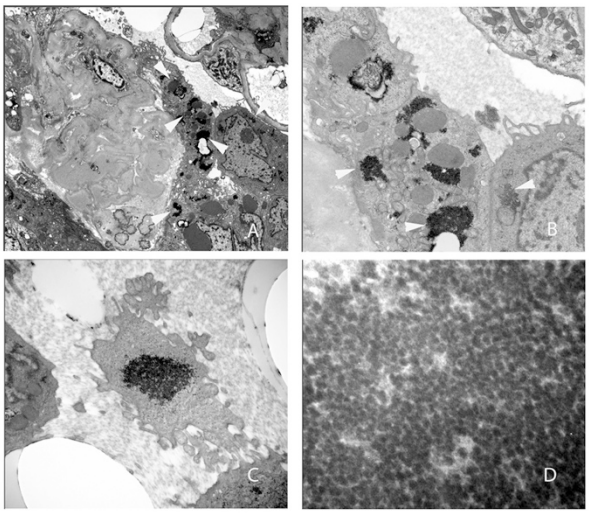

Conclusions: Although HIV particles are rarely identified in podocytes in HIVAN, HIV-1 virus may directly infect, survive and replicate in the podocytes and cause podocyte injury. Both viral protein and directly viral infection may responsible for podocytopathy and characteristic pathologic changes of collapsing of glomerular tufts in HIVAN.

2122 Immunotactoid Glomerulopathy (ITG) and Cryoglobulinemic Nephropathy (CN) – A Unifying Conceptual Approach

Guillermo Herrera, Kunle Ojemakinde, Elba Turbat-Herrera, Xu Zeng, Samy Iskandar. Louisiana State University Health Sciences Center, Shreveport, LA; Temple University School of Medicine, Philadelphia, PA; Wake Forest School of Medicine, Winston-Salem, NC.

Background: Among the entities with organized deposits one of the most intriguing is immunotactoid glomerulopathy (ITG). Initially considered to be the same as fibrillary glomerulonephritis, it is clear now that these are two completely distinct entities.

One important association is that of ITG with underlying neoplastic monoclonal processes such as lymphoproliferative disorders and MGUS. Interestingly, though not as frequently, the same is true for CN.

One of the main differential diagnosis of ITG is CN because of the similarity of the organized deposits (in both there are microtubular aggregates) and overlap in the diameter of the microtubules.

Design: 50 CN were compared with 7 ITG cases with emphasis on light and electron microscopic findings and correlation with immunofluorescence data. Clinical histories were reviewed. Renal biopsies were routinely handled for light, immunofluorescence and ultrastructural evaluation.

Results: Clinically, ITG and CN shared numerous features, including the presence of underlying lymphoproliferative disorders, though found more commonly in ITG. Prognosis and clinical behavior were also rather similar.

Both entities were characterized by deposits composed of microtubules. The diameter of the microtubules in CN ranged from 15-30 nm and in ITG up to 60 nm but mostly 25-45 nm. While the finding of microtubules in capillary thrombi in CN was a common finding (in 30% of patients), there were also aggregates of microtubular structures in capillary thrombi in 2 of the 7 IG cases. Five of 7 ITG and 10% of CN cases were light chain-restricted. Two ITG cases had circulating cryoglobulins. The diameter and appearance of the microtubules in CN cases overlapped with those of ITG; however, the latter were generally thicker and tended to align in a parallel arrangement.

Conclusions: The finding of microtubular structures in capillary thrombi in some ITG cases suggests that a circulating protein participates in its pathogenesis and the fact that the majority of these cases are associated with a monoclonal process supports that a monoclonal cryoglobulin may be involved. We postulate that the entities currently recognized ITG and CN fall within the spectrum of renal manifestations in cryoglobulinemia; therefore, ITG should be considered a morphologic variant of CN.

2123 Primitive Myxoid Mesenchymal Tumor of Infancy: Review of Histopathologic and Ultrastructural Features

John Hicks. Texas Children's Hospital & Baylor College of Medicine, Houston, TX.

Background: PMMTI is a rare soft tissue neoplasm first described in 2006. It is a focally aggressive mesenchymal tumor that represents the primitive end of the spectrum of fibroblastic-myofibroblastic tumors. It is composed of primitive spindled cells in a myxoid background. PMMTI usually occurs during the 1st year of life and has a long, indolent course complicated by fre-quent relapses, PMMTI is a locally aggressive tumor with a proclivity to recur and has a high level of resistance to chemotherapy, Only 10 cases have been reported in the literature since this entity was first recognized as a distinct entity.

Design: The surgical and consultative pathology archives were searched for myxoid tumors arising in children less than 5 years of age. The study population consisted of 3 females and 2 males ranging in age from 2 to 14 mos of age. The sites of involvement were hard palate, neck, thigh, chest wall and scalp. All children underwent surgical resection with local recurrence in 4 of the 5 children. There was no evidence of metastatic disease in any children. Tissue was available for histopathologic and ultrastructural evaluation.

Results: All tumors had homogenous myxoid gray-tan cut surfaces and showed local infiltration and multinodular growth without encapsulation. Tumor size ranged form 6 to 20 cm. Tumors were composed of primitive round to polygonal to spindled mesenchymal cells with bland, uniform nuclei with fine, homogenous chromatin, and amphophilic to lightly eosinophilic cytoplasm. Tumor cells are embedded in a diffuse myxoid background with a delicate vascular network. The cellularity was low to moderate with an occasional focal herringbone pattern. The mi-totic rate was variable. Immunohistochemistry showed only diffuse positivity for vimentin. Electron microscopy highlighted the primitive nature of the mesenchymal cells with no differentiation and abundant myxoid stroma. Cytogenetic (n=5) and molecular genetic (n=3) studies revealed absence of t(12;15) ETV6- NTRK3 fusion and no mutations in CTNNB1 gene (n=3), eliminating infantile fibrosarcoma and desmoid fi-bromatosis, respectively.

Conclusions: PMMTI is a rare primitive mesenchymal tumor predominantly occurring in infancy and is important to differentiate from other myofibroblastic and fibroblastic tumors of infancy due to the need for complete surgical excision to avoid recurrence and its resistance to chemotherapeutic management. Diagnosis usually requires a multimodal approach to eliminate other soft tissue tumors that occur in infancy.

2124 Role of Scanning Electron Microscopy in Diagnosis of Hair Shaft Abnormalities

John Hicks. Texas Children's Hospital, Houston, TX.

Background: Hair shaft abnormalities may be acquired or congenital. Clinical examination shows changes in color, density, and length. Hair shaft disorders are secondary to structural alterations in hair fibers and cuticles, leading to brittle, dry and lusterless hair. Although, light microscopy may identify certain features such as alternating light and dark bands (tiger tail pattern) seen in certain conditions, scanning electron microscopy (SEM) rapidly identifies hair shaft abnormalities. Hair shaft abnormalities may be the 1st sign of an underlying syndrome requiring genetic evaluation.

Design: Anatomic pathology archives were searched for hair shaft abnormalities examined by SEM over a 5 year period. A total of 44 cases were identified.

Results: Pili canaliculi et trianguli (PCT) was identified in 19 cases, and characterized by longitudinal grooving and triangular or heart-shaped appearance on cross-section. Familial cases with autosomal dominant inheritance may occur. Associated abnormalities include cataracts, abnormal bone development, alopecia areata and lichen sclerosus. Pili torti (PT) was identified in 9 cases and characterized by hair shafts with twisting and flattening. Fractures may occur at twist areas. PT is associated with unruly thin fragile hair of eyebrows, eyelashes and scalp. It may be associated with nonprogressive mental deficiency, sensorineural hearing loss, hypogonadism, ectodermal dysplasia, Menkes and GRACILE syndromes, citrullinemia, and other hair shaft abnormalities. Trichorrhexis nodosa was identified in 8 cases and characterized by beaded nodal areas along hair shafts with fraying and fracturing. This disorder may be genetic (arginosuccinicaciduria, citrullinemia) or acquired. Trichoschisis was identified with 3 cases, and characterized by impending "clean" breaks in the hair shafts. This condition may be associated with trichothiodystrophy (TTD) with brittle hair and low sulfur content. TTD is an autosomal recessive neuroectodermal disorder with 8 subgroups, and has impaired DNA repair. Atrophy with markedly decreased diameters were noted in 5 cases.

Conclusions: SEM rapidly identifies abnormalities with many hair shaft disorders, allowing for appropriate categorization. Definitively diagnosing hair shaft disorders is important in guiding appropriate clinical evaluation and genetic testing to determine if an underlying genetic defect is responsible for the hair shaft abnormality. Detection of hair shaft disorders may allow for early diagnosis of an associated syndrome, allow for appropriate treatment interventions, anticipate medical conditions that may develop, and predict prognosis.

2125 Tubular Aggregate Myopathy: Ultrastructural Features

John Hicks. Texas Children's Hospital, Houston, TX.

Background: Tubular aggregate myopathy (TAM) is a rare disease that was first described in 1964 and represents 0.2% of all muscle biopsies. Both sporadic and familial cases have been described, with several familial cases with autosomal dominant and recesive patterns.TAM is more common in males than females and has a wide age range (2-55 years). TAM presents as exercised-induced muscle pain, cramps and stiffness with easy fatiguability, and is a slowly progressive disease with severe disability. Tubular aggregates identifed by electron microscopy are the diagnostic hallmark, and most likely originate from the terminal cistern of the sarcoplasmic reticulum.

Design: The electron microscopy pathology referral case archives were searched for potential cases of TAM. Three cases were identified and these cases had only had tissue submitted for electron microscopy. There were 3 children (2 males:1 female) with an age range of 2 to 6 years. The semi-thin toluidine blue fuchsin stained glass slides and electron micrographs were available for review.

Results: All cases showed characteristic tubular aggregates to a variable degree. Several different patterns were noted, including vesicular membrane pattern, single wall tubule pattern, double wall tubule pattern and dilated tubules with inner tubule pattern. The tubules were most often the characteristic 60-70 nm in diameter with the vesicular membrane pattern having tubules ranging from 60 to 300nm in diameter. There were no significant other myofilament or mitochondrial abnormalities. No evidence of metabolic inclusion disease was identified. Based upon the ultastructural features, additional genetic testing at the originating institutions identified STIM1 (n=2, Stormorken syndrome) and ORAI1 (n=1, Stormorken-like syndrome) gene mutations.

Conclusions: Ultrastructural discovery alone of tubular aggregates in individuals with myopathic symptoms proved to be the essential element in diagnosing a rare myopathy (TAM). This further lead to genetic testing allowing for identification of syndromes associated with TAM (Stormorken [STIM1] and Stormorken-like [ORAI1]

syndromes). The diagnostic tubular aggregates most likely originate from the terminal cisterns of the sacroplasmic reticulum (SR). These aggregates contain SR proteins – RYR, triadin, calsequesterin, sacralumenin, sarcoplasmic endoplasmic calcium ATPase, dihydropyridine receptor. Tubular aggregates result in sarcoplasmic calcium homeostasis disturbance.

2126 Ultrastructural Correlation of Cytological and Fluid Diagnosis: A Useful Adjunct To the Diagnostic Algorithm in Difficult Cases

Ipshita Kak, Monalisa Sur, Rakhshinder Parmar, Clara Nguyen, Jorge Arredondo. McMaster University, Hamilton, ON, Canada; Juravinski Hospital, Hamilton, ON, Canada; St. Joseph's Healthcare Hamilton, Hamilton, ON, Canada; McMaster University Medical Centre, Hamilton, ON, Canada.

Background: In an age where most laboratories are challenged to provide a faster, accurate and cost-effective means of rendering a diagnosis, cytology yields an opportunity to fulfill these demands and effectively direct patient management. However, in cases where ancillary techniques are required to provide a more specific answer, appropriate specimen utilization becomes crucial. Despite studies demonstrating electron microscopy's ability to facilitate accurate diagnosis in cytology in 47.4 - 81% cases, it continues to remain an underutilized auxiliary test.

Design: Cases for this study included pleural, peritoneal or pericardial effusions assigned to the co-investigator pathologist. Evident positive malignancy on cytology with adequate unfixed fluid sample left after regular cytology process were selected. Based on the protocol approved by REB, 30 mL of the remainder fluid was centrifuged for 10 minutes at 4000 rpm. The pellet obtained was resuspended in 1.5 mL of glutaraldehyde and transferred to an eppendorf tube. Samples were sent to the EM Lab (with a unique study number for anonymity) and handled with a standard process. Digital images obtained were reviewed and interpreted by the principal investigator and co-investigator who were blinded to the cytological diagnosis .

Results: Out of 8 cases sent to electron microscopy, 2 did not have the representative tumor on the EM section when compared to the cytology slides, demonstrating the limitation in interpretation, thus serving as an important internal quality assurance. Six cases were correlated for final diagnosis based on EM and cytology and showed a 83.3% (5/6) concordance rate. The singular case that did not correlate contained scant amount of tumor cells on the EM slide which could explain the discrepancy in result. Additional cases are in the process of being prospectively obtained and added to the study.

Conclusions: Preliminary results from this pilot study demonstrate that electron microscopy shows a robust concordance with the diagnosis obtained from routine cytology and current ancillary testing. This gives credence to our hypothesis that electron microscopy could serve as a valuable ancillary test in the analytical framework of cytology cases, especially in challenging scenarios.

2127 Ultrastructural Evaluation Confirms Surfactant Dysfunction Disorder Associated With a Previously Unclassified Heterozygous Variant in ABCA3 [c.863G>A (p.Arg288Lys)]

M Kamran Mirza, Elizabeth Sengupta, Renukadas Sakalkale, David Mowat, Aliya Husain. University of Chicago, Chicago, IL; Sydney Children's and Prince of Wales Hospitals, Sydney, Australia.

Background: More and more mutations/genetic defects are being described as cause of respiratory distress syndrome (RDS) due to surfactant dysfunction disorders (SDD), the most common of which is *ABCA3* mutation. Here we report the utility of ultrastructural microscopy in confirming a previously unclassified variant of ABCA3 [c.863G>A (p.Arg288Lys)] that led to surfactant dysfunction, respiratory distress and ultimately death of the patient.

Design: Electron microscopy was performed on a deparaffinized section of formalin fixed lung wedge biopsy. Mutation analysis was performed for the following: *SFTPB*, *SFTPC*, *ABCA3* and *NKX2* genes.

Results: A baby girl born at 34 weeks' gestation had virtually no respiratory effort at birth and was managed with ventilation. She was unable to be weaned off high-frequency ventilation despite surfactant therapy. A CT scan performed at 1 week of age (35 weeks corrected gestational age) showed patchy areas of atelectasis in the right upper lobe and subsegmental atelectasis of the superior segment of the left lower lobe. Biopsy at day 52 of life showed well expanded lung sections with diffuse alveolar architectural abnormality. The airways were simplified, moderately enlarged with rounded contours. There was diffuse but mild interstitial widening and extensive type II pneumocyte hyperplasia. Molecular analysis for *ABCA3* revealed heterozygosity for a known variant, c.863G>A (p.Arg288Lys), in exon 8 of the ABCA3 gene, that was thought to be non-pathogenic. Ultrastructural examination demonstrated marked decrease of surfactant granules, with one granule showing electron dense material, and a diagnosis of SDD was rendered.

Conclusions: ABCA3 [c.863G>A (p.Arg288Lys)] has been reported in a compound heterozygote state, with other ABCA3 variants, in two different families with RDS (Brasch et al. 2006, Am J Respir Crit Care Med 174:571-580). Furthermore, it has also been reported in a young boy with acute febrile respiratory infection, also in a compound heterozygous state with another ABCA3 variant (Copertino et al. 2012, Arch Bronconeumol 48(4):139-140). Although, in silico analysis (Alamutv2.3) using Align GVGD, SIFT, PolyPhen and Mutation Taster all suggest this variant to not be pathogenic, however, ultrastructural evaluation confirmed an SDD phenotype without a compound heterozygous state in the patient reported here.

2128 Adrenal Gland Inclusions in Patients Treated With Aldosterone Antagonists (Spironolactone/Eplerenone): Incidence, Morphology, and Ultrastructural Findings

Kishan Patel, Edward Calomeni, Tibor Nadasdy, Debra Zynger. Ohio State University Medical Center, Columbus, OH.

Background: Spironolactone is often used to treat hypertension caused by hyperaldosteronism, and as a result, can form concentrically laminated electron dense spironolactone body inclusions within the adrenal gland. Spironolactone bodies have not been investigated in a contemporary cohort or in patients treated with the more recently approved aldosterone antagonist, eplerenone.

Design: Spironolactone bodies were retrospectively investigated in patients treated for hyperaldosteronism (n = 15) from 2012-2013 that underwent a subsequent adrenalectomy.

Results: Inclusions were identified in 33% of patients treated with aldosterone antagonists, far less than previously reported. Remarkably, 50% of patients treated with spironolactone had inclusions while no patients using eplerenone alone had inclusions. Two patients treated with spironolactone had bodies present longer than the duration described in prior studies. Inclusions unexpectedly persisted in 1 patient despite increased duration of discontinued pharmacological treatment. A spectrum of histologic and ultrastructural findings were encountered within an adrenal cortical adenoma from a patient treated with both spironolactone and eplerenone. Ultrastructural examination revealed laminated electron dense bodies with the appearance of classic spironolactone inclusions as well as electron dense bodies without laminations and laminated bodies without electron dense cores.

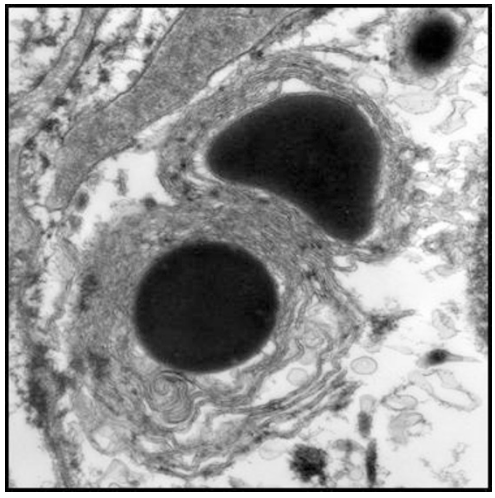

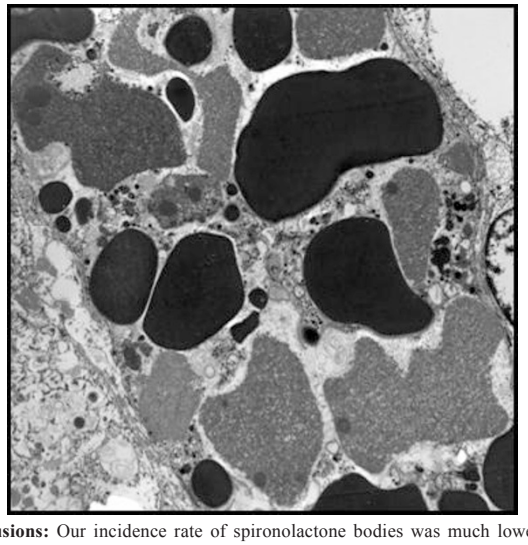

Conclusions: Our incidence rate of spironolactone bodies was much lower than previously reported, with no inclusions seen in patients treated solely with the newer aldosterone antagonist, eplerenone. Pathologists should be aware of these infrequently encountered inclusions, particularly as the clinical history of hyperaldosteronism and pharmacologic treatment may not be provided.